Wideband Surface Impedance Measurements in Superconducting Films.

Enrico Silva, *Member, IEEE,* Nicola Pompeo, *Member, IEEE,* Kostiantyn Torokhtii, *Member, IEEE,* and Stefano Sarti

***Abstract*—We discuss calibration issues in wideband (2-20 GHz) surface impedance measurements in a cryogenic and high-magnetic-field environment. We show that, in the case of measurements taken on superconducting thin films, the substantial impossibility of a full, three-standard calibration can be partially overcome by exploiting appropriate approximations and the basic properties of superconductors. We discuss a modification of the so-called "short-only" calibration, in order to increase the accuracy of the measurements. We relate the material properties of a sample under study to the measured surface impedance, which is affected by the geometry of the measurement, and we discuss the effects on the proposed approximate calibration procedure. We check experimentally the applicability of the approximations at the ground of the method, and we discuss thoroughly the uncertainties related to the approximations employed. Finally, we report sample measurements of the surface impedance of two MgB_2 superconducting films.**

***Index Terms*—**

I. Introduction

Radio frequency and microwave measurement techniques for the investigation of material properties [1] are of tremendous interest in many fields involving both applications and fundamental research: they are used to measure the complex permittivity of dielectrics [2], [3], of interest for biomedical applications [4], [5], for telecommunications [6], for geological exploration [7], as reference materials in the calibration and standardization of the measurements systems [8]. In the study and characterization of magnetic materials, they enable the measurement of the complex permeabilityof, e.g. ferrites used in microwave circuitry [9] and electromagnetic absorbers used in communication systems [10]. Finally, they are also exploited in the determination of electrical transport properties of various conducting materials, such as in the non-destructive resistivity mapping of semiconductors [11], in the complex conductivity σ measurements of conductive engineered composites [12] and in the study and characterization of superconductors [13]–[22].

The microwave techniques fall broadly in two classes: resonant and wideband. We are here interested on the latter: the sample to be measured is placed within a waveguide or coaxial structure, or even in free space, and the electromagnetic wave transmission and/or reflection through/from the sample are measured, ultimately yielding the surface impedance of the sample in a wide range of frequencies.

K. Torokhtii, N. Pompeo and E. Silva are with Dipartimento di Ingegneria, Università Roma Tre, Via della Vasca Navale 84, 00146 Roma, Italy. Email: enrico.silva@uniroma3.it.

S. Sarti is with Dipartimento di Fisica, Sapienza Università di Roma, Roma, Italy.

The definition of "wideband" is rather fuzzy: in some cases a range covering a single waveguide band is considered to be wideband, while in other cases several decades in frequency are considered. In this paper we focus on the wideband Corbino disk technique, tailored in the specific case for the complex conductivity measurement of superconducting thin films. We have developed and recently presented [23] a technique capable to assess the properties of the sample under study at least in the range 1–20 GHz. Similarly to other realizations [17]–[22], the method is based on the measurement of the complex reflection coefficient Γ_m at the input of a coaxial line terminated by the film (Corbino disk). Since a coaxial structure, contrary to waveguides, supports TEM modes, the operative frequency range spans in principle between d.c. and the cutoff frequency of the cable. The technique is conceptually the same as the so-called open-ended coaxial probe largely used in the permittivity measurement of liquids [24], but two main important differences justify the specific treatment to the case of conducting samples. First, a good electrical contact between the coaxial probe and the sample is fundamental, whereas on liquids this problem is simply absent. Second, the measurement of high conductivity materials in a cryogenic environment makes the essential aspect of the calibration of the line a very complicate, and somehow non fully solvable, problem.

Aim of the technique is to obtain measurements of the complex resistivity $\tilde{\rho}$ (or complex conductivity $\tilde{\sigma} = 1/\tilde{\rho}$) of a superconducting sample, in the shape of a thin film deposited on a suitable dielectric substrate. Thus, the determination of the sample complex resistivity requires several distinct and specific steps: first, the reflection coefficient at the sample location Γ_0 must be obtained from the measured reflection coefficient through a proper calibration of the line contribution. Then, the effective complex surface impedance $Z = R + \mathrm{i}X$ [25] of the sample, depending essentially on its complex conductivity and thickness, is derived according to the textbook expression [26]:

$$Z(\nu) = Z_0 \frac{1 + \Gamma_0(\nu)}{1 - \Gamma_0(\nu)} \tag{1}$$

where Z_0 is the characteristic impedance of the line and ν is the measurement frequency. Finally, the complex resistivity $\tilde{\rho}$ must be related to the effective complex surface impedance Z, which is strongly affected by the geometry of the sample.

The various issues involved in the entire procedure are addressed in the paper as follows. In Sec. II we define the measurand Z and the relation with the material property $\tilde{\rho}$ in the Corbino disk geometry, including some useful ap-

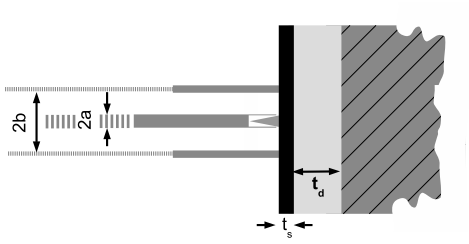

Fig. 1. Graphical sketch of the geometry at the boundary between the connector and the sample under study.

proximations and the estimate of the deviations occurring in their use. In order to focus the main issues in a practical environment, we describe in Sec. III a typical experimental setup. In Sec. IV we address the approximations involved in the partial calibration proposed, and we thoroughly discuss and estimate the uncertainties involved. In Sec. V we present experimental data to check the approximations used, as well as sample experimental data for the surface impedance of superconducting MgB_2 samples. In Sec. VI we summarize and conclude.

II. The measurand and the material property

The present work is focused on the wideband measurements of superconducting materials, in the shape of thin films. The effective surface impedance Z (or, as we will see later, its variation with an external parameter) is the desired measurand. However, it is related in a nontrivial way to the material property, $\tilde{\rho}$. Thus, there is the need to investigate the relation between $\tilde{\rho}$, Z and Γ_0. Eq. (1) relates the reflection coefficient at the sample surface to the effective surface impedance. We will show in Sec. IV that the specific properties of superconductors are of paramount importance in the approximate calibration procedure that we propose, in order to relate the measured (at the location of the VNA, Vector Network Analyzer) reflection coefficient to Γ_0. In the present Section we explore the connections between Z and $\tilde{\rho}$. In doing so, it will be useful to state the results in terms of the surface admittance, $Y = Z^{-1}$.

The structure under study is a thin superconducting film, of thickness t_s, deposited onto a dielectric substrate of thickness t_d, and backed by a metal block (See Fig.1). It is possible to model the conducting structure as laterally infinite [27]. The structure to analyze becomes then a coaxial line in contact with a laterally infinite (super)conducting film/dielectric/metal (the so-called "open ended" geometry). In this case, the effective admittance Y has been calculated [27]. The result can be cast in the following compact form:

$$Y = \int_0^{+\infty} K(\zeta, k_0) Y_{eff}(\zeta) d\zeta \tag{2}$$

where $K(\zeta, k_0) = [J_0(k_0 b\zeta) - J_0(k_0 a\zeta)]^2/[\zeta \ln(b/a)]$, J_0 is the zeroth-order Bessel function, a (b) is the inner (outer) radius of the coaxial line, and $\int_0^\infty K(\zeta, k_0) d\zeta = 1$. Eq. (2) contains implicitly all the complications of the layered structure. Let us indicate with $j = s, d, m$ the index of the material involved (superconductor, dielectric substrate, metal backplate, respectively). For each material one writes:

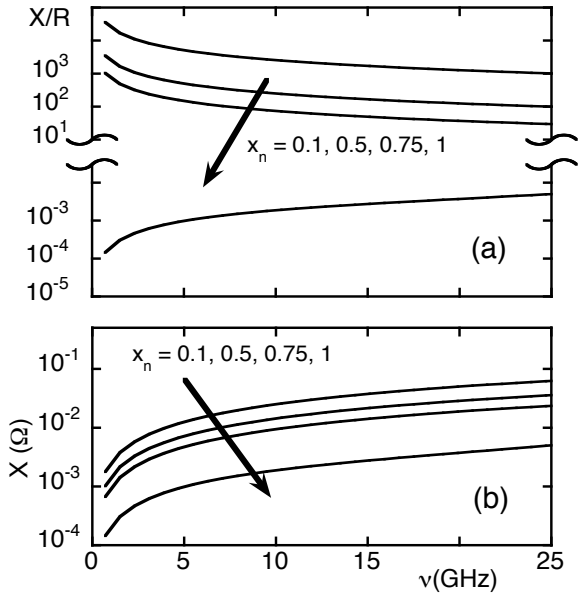

Fig. 2. (a) Ratio of the effective surface reactance and resistance, X/R, in a typical superconducting film (see main text): it is evident that, in the normal state ($x_n = 1$), the imaginary part is negligible in the frequency range under scrutiny. (b) Effective surface reactance X vs ν: it is immediately seen that $X \ll Z_0$; together with $X/R \gg 1$, panel (a), it validates $\Gamma_0 \simeq -1$ in the superconducting state.

$$Y_j(\zeta) = \omega \epsilon_0 \tilde{\epsilon}_j / k_j(\zeta) \tag{3}$$

$$k_j(\zeta) = k_0 \sqrt{\tilde{\epsilon}_j - \zeta^2} \tag{4}$$

$$\tilde{\epsilon}_j = \epsilon'_j + \mathrm{i}\epsilon''_j - \mathrm{i}\frac{1}{\epsilon_0 \rho_j \omega} \tag{5}$$

where $k_0 = \omega/c$, $c = 1/\sqrt{\epsilon_0 \mu_0}$ is the speed of light in vacuum, ϵ_0 is the permittivity of the vacuum, $\omega = 2\pi\nu$ is the angular frequency, and $\epsilon'_j + \mathrm{i}\epsilon''_j$ and ρ_j are the relative complex permittivity and the resistivity of the material "j", respectively. In our geometry, for Y_{eff} one has [27], [28]:

$$Y_{eff}(\zeta) = Y_s(\zeta) \frac{\bar{Y}_d(\zeta) + \mathrm{i} Y_s(\zeta) \tan[k_s(\zeta) t_s]}{Y_s(\zeta) + \mathrm{i} \bar{Y}_d(\zeta) \tan[k_s(\zeta) t_s]} \tag{6}$$

$$\bar{Y}_d(\zeta) = Y_d(\zeta) \frac{Y_m(\zeta) + \mathrm{i} Y_d(\zeta) \tan[k_d(\zeta) t_d]}{Y_d(\zeta) + \mathrm{i} Y_m(\zeta) \tan[k_d(\zeta) t_d]} \tag{7}$$

We will make use of Eq. (2) to obtain Z. We note that the effect of the substrate can affect strongly Y_{eff} [29]. However, in the present case several useful simplifications of the rather complex Eq. (2) take place: if the film is sufficiently thin, so that $|k_s t_s| \ll 1$, one can approximate $\tan[k_s(\zeta) t_s] \simeq k_s(\zeta) t_s$; if the substrate is insulating, one usually finds $\bar{Y}_d \ll Y_s$ (in very large permittivity dielectrics this is not fullfilled at specific frequencies [30]); in Eq. (5) one can neglect $\epsilon'_j + \mathrm{i}\epsilon''_j$ for the s and m materials, and $\epsilon''_j - 1/\epsilon_0 \rho_j \omega$ in a typical dielectric employed as a substrate. Using these approximations, it is possible to show that

$$Y \simeq \mathrm{i}\omega \epsilon_0 \tilde{\epsilon}_s t_s + \int_0^\infty K(\zeta, k_0) \bar{Y}_d(\zeta) d\zeta \tag{8}$$

Since we are dealing with superconducting materials, one finds two important properties that will prove useful in the calibration procedure (Sec. IV). First, in the normal state ρ_s is real [31], so that in Eq.(8) $\mathrm{i}\omega\epsilon_0\tilde{\epsilon}_s t_s = t_s/\rho_s$. Second, deep in the superconducting state $\rho_s \simeq \mathrm{i}\omega\mu_0\lambda^2$, where the London penetration depth $\lambda \sim 50 \div 500$ nm [31]. One then has $\tilde{\epsilon}_s \simeq -(c/\omega\lambda)^2 \gg 1$, and with some algebra one gets:

$$Y \simeq \mathrm{i}\frac{1}{\omega\mu_0\lambda}\tanh\frac{t_s}{\lambda} \tag{9}$$

Eq. (9) has the immediate important result (see Sec. IV) that deep in the superconducting state, since $|Y| \gg Y_0 = Z_0^{-1}$ (or, which is the same since $X \gg R$, $X \ll Z_0$), Eq. (1) yields $\Gamma_0 \simeq -1$.

To illustrate the preceding properties, we present in Fig. 2 a subset of the simulations of Z, obtained with the following parameters: $t_d = 0.5$ mm, $\tilde{\epsilon}_d = 9$, $t_s = 150$ nm, $\rho_{s,n} = 3{\cdot}10^{-7}\Omega{\cdot}$m (in the normal state), $\lambda = 150$ nm. We took for illustrative purposes the two–fluid model [31]: $\rho_s = [x_n/\rho_{s,n} - \mathrm{i}(1-x_n)/\omega\mu_0\lambda^2]^{-1}$, where $x_n \in [0,1]$ describes the transition from a normal ($x_n = 1$) to a superconducting ($x_n = 0$) state. As it can be seen, the calculations fully support the results here depicted.

III. Experimental setup

The calibration scheme that we propose is intended to apply to a *cryogenic* line (temperatures T down to 3 K), in presence of *strong magnetic fields* ($\mu_0 H \leq$14 T). The ultimate goal is to obtain measurements of the complex conductivity (or of the complex resistivity) of a thin superconducting film as a function of the temperature, applied magnetic field, and frequency. It is clear that such requirements are particularly challenging with respect to the calibration of a coaxial line.

The scheme of the measurement apparatus used in Sec. V is provided in Figure 3. The temperature is varied by controlling the liquid Helium flow, and the magnetic field is supplied by a superconducting solenoid. The VNA is connected to the sample by a commercial coaxial cable (cutoff frequency: 60 GHz), terminated on the sample by a double-spring, custom-made connection [19] using a launcher and a tiny, cone-shaped pin inserted in the center conductor of the launcher: a good contact between the terminal section of the coaxial cable and the sample under test is critical in order to minimize the parasitic contact impedance (mainly resistive and capacitive). The need for stable electrical contact between room temperature T_r and cryogenic temperatures (down to $T_{min} \sim 3$ K) dictates the technical solution. Of course, all the assembly (line, connectors, etc) has to be nonmagnetic up to 14 T.

The features necessary to operate in a cryomagnetic environment affect heavily the properties of the line, and ultimately the feasibility of an accurate calibration. First, the temperature is varied at the sample location: different sample temperatures produce different temperature gradients, and different responses of the line. Second, the high magnetic field requires that the VNA is placed far from the cryostat. The microwave line is thus very long (1 meter inside the cryostat and 2.5 meters outside), with deleterious effects on the attenuation, on the noise and on the phase stability. Finally, the double-spring

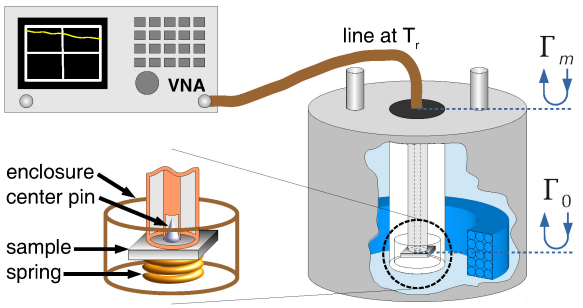

Fig. 3. Scheme of the measurement apparatus and of the custom–made connector.

connector does not completely solve the issue of parasitic capacitance, acting as a high–pass on the signal. As a result, measurements above 35 GHz and below 1 GHz are basically unreliable, and rather noisy above 20 GHz. The use of a 60 GHz cable is however justified: the small cable ensures less heat transfer to the sample. Moreover, pure TEM wave is ensured by the very high cutoff frequency.

The desired measurand, Z, is linked to the complex reflection coefficient measured at the VNA location. Two kinds of measurements can be made during a measuring session: the collection of a set of curves at fixed magnetic field H_0 and different temperatures T, $Z(\nu;T,H_0)$ ("temperature sweeps"), or at different magnetic fields H and fixed temperature T_0, $Z(\nu;T_0,H)$ ("field sweeps"). The dependencies on ν, T, H will be often omitted in the following for the sake of compactness.

IV. Calibration of the cryogenic line

A. The problem

As anticipated in the introduction, the main problem dealt with in this paper is how to extract the surface impedance $Z(\nu)$ of the sample from the reflection coefficients $\Gamma_m(\nu)$ measured at the beginning of the coaxial cable. In principle, $\Gamma_0(\nu)$ can be extracted from the measured $\Gamma_m(\nu)$ through the standard relation [25], [26]:

$$\Gamma_m = S_{11} + \frac{S_{21}S_{12}\Gamma_0}{1 - S_{22}\Gamma_0} \tag{10}$$

where S_{ij} are the scattering coefficients of the line[1]. In the ideal case, $S_{11} = S_{22} = 0$ and $S_{12} = S_{21} = 1$. For the analysis that will follow, a very relevant feature of Eq.(10) resides in the fact that the forward and reverse trasmission coefficients, S_{12} and S_{21}, do not appear individually, but only as a product. The immediate consequence is that, in order to describe the line behaviour in this situation, where the measurement is performed at the port 1 of the line and the load is connected at the port 2 of the line, only *three* parameters need to be determined: S_{11}, S_{22} and the *product* $S_{21}S_{12}$. The full one–port line calibration requires their determination by measuring the response of three accurately known loads, typically a short, an open and a matched load. This is feasible

[1]For the ease of comparison with the literature, we remark that in this context one often finds the notation E_d, E_s, E_r instead of S_{11}, S_{22}, $S_{21}S_{12}$, respectively [17]–[21].

for the portion of the line between the VNA and the cryostat: this segment can be fully calibrated with the standard method, and its contribution then fully accounted for. Operatively, this is done, following the standard procedure, by storing these calibration coefficients in the VNA memory and by instructing the VNA to directly apply the calibration correction to the subsequent measurements. Proceeding with care, within a well thermalized environment in the laboratory, a daily calibration of the line connecting the cryostat to the VNA is sufficient and commonly done. However, the cryogenic part of the line cannot be easily calibrated in such a standard fashion, for several reasons. First, the "calibration standards", which require accurate construction, characterization and modelling, are available at room temperature only. Second, the scattering coefficients of the cryogenic line depend on the sample temperature and temperature profile of the whole cable (even if, with the proper nonmagnetic choice for the assembly, they do not depend on magnetic field). The latter is highly nonreproducible. Thus, a full calibration of a cryogenic line in a practical environment is not feasible. In particular, one should note that the issue related to the temperature profile are particularly deleterious for the reproducibility of the *phase* of the cable assembly. We will show that this aspect affects mostly the accuracy of the measurement of the surface reactance X.

In order to cope with this issue, various approaches have been devised and followed. In Ref. [17], a weak temperature dependence was assumed for S_{11} and S_{22}, that could be obtained by a full calibration at T_r. Then, by using a reference measurement at cryogenic temperature performed on the same superconducting sample to be measured, the product $S_{21}S_{12}$ was recomputed at low T obtaining an approximate cryogenic recalibration ("short–only" calibration [20]). Alternatively, three custom standards were built [18], [20], [21], inevitably of lower quality than those used in metrology and for laboratory grade VNA calibrations. Then, a lengthy (three distinct cool-down) full calibration of the line (with great attention in keeping a highly reproducible T gradient) could be performed. The need for an appropriate cryogenic calibration is a widespread issue, that becomes even more complex when two-port devices have to be probed. In this context, alternate approaches have been developed [32], [33]. However, in most cases involving the one–port calibration, it was observed that, when dealing with superconductors, a measurement performed on the sample under study at a reference T ensured better error corrections.

The main issues concern mostly the phase of the line scattering coefficients, which is extremely sensitive to the temperature distribution on the entire coaxial line and to the contact impedance between the coaxial probe and the sample or the standards. Given the complexity of the system, both the T distribution and the contact impedance suffer from reproducibility issues despite the strenuous efforts spent in that direction. Thus, whenever feasible, a reference measurement on the sample itself proves to be a superior calibration since it ensures identical contact between the two measurements and the same thermal condition on the line. This choice obviously limits the application of this kind of calibration to the cases where the sample itself presents a substantial change in the reflection coefficient, driven by some external parameter (a superconductor is the most evident example): it is essential that the sample remains *in situ*, any removal of the sample would void the reliability of this technique. We describe in the following our contribution to the improvement of this procedure, providing a discussion and an evaluation of the uncertainties involved in the measurement and calibration process.

B. Partially calibrated reflection coefficient $\widetilde{\Gamma}_0(\nu)$

The basic idea is to proceed by incremental calibrations with suitable approximations. At the beginning of the experiment we determine the scattering coefficients S_{11}, S_{22} and the product $S_{21}S_{12}$ of the internal cable at room temperature T_r, by performing the standard one–port calibration: three "calibrated", i.e. with the calibration correction for the outer line directly applied, measurements of Γ_m are performed by placing at the lower end of the inner cable the three calibration standards (load, short and open) after having removed the final launcher, which constitutes the Corbino connector. This step implies that the Corbino connector is inevitably not accounted for in the calibration scheme. Using Eq. (10), we define a partially calibrated reflection coefficient $\widetilde{\Gamma}_0(\nu;T)$ as (we omit the explicit frequency dependence for the sake of compactness):

$$\widetilde{\Gamma}_0(T) = \frac{\Gamma_m(T) - S_{11}(T_r)}{S_{21}(T_r)S_{12}(T_r) + S_{22}(T_r)\left(\Gamma_m(T) - S_{11}(T_r)\right)}. \tag{11}$$

The uncertainty $u(\widetilde{\Gamma}_0)$ can be derived from the uncertainties on Γ_m and S_{11}, S_{22} and $S_{21}S_{12}$ as a standard combined uncertainty [34], [35]. The uncertainty $u(\Gamma_m)$ on the (complex) quantity Γ_m, which is a VNA *calibrated* measurement (it includes the calibration of the coaxial line outside of the cryostat) is provided by the manufacturer as a function of ν and of $|\Gamma_m|$. For frequencies $\nu \leq 20$ GHz, and for high $|\Gamma_m|$ (we are considering conductive samples), $u(|\Gamma_m|) = 0.005$–0.02 and $u(Arg(\Gamma_m)) = 0.01$–0.02 rad [36]. The room–temperature scattering coefficients S_{11}, S_{22} and $S_{21}S_{12}$ of the inner line are computed performing three room temperature *calibrated* measurements $\Gamma_{m,S|O|L}$, with the calibration standard Short, Open and Load, respectively, at the lower end of the inner coaxial line. Hence $u(\Gamma_{m,S|O|L})$ is conceptually the same as $u(\Gamma_m)$. Since $|\Gamma_{m,S|O}| \simeq 1$ and $\Gamma_{m,L} \simeq 0$, $u(\Gamma_{m,S|O}) = u(\Gamma_m)$ and $u(|\Gamma_{m,L}|) = 0.008$ [36]. Propagating the uncertainties to S_{11}, S_{22} and $S_{21}S_{12}$ [37]–[39] and ultimately to $\widetilde{\Gamma}_0$, the computation yields $u(|\widetilde{\Gamma}_m|) = 0.008$–$0.03$ and $u(Arg(\widetilde{\Gamma}_m)) = 0.016$–$0.032$ rad. We discuss in the following the additional terms and the role of the approximations.

If the scattering coefficients were temperature independent, Eq. (11) would yield Γ_0. Putting Eq. (10) into Eq. (11) one has:

$$\Gamma_0(T) = \frac{D(\widetilde{\Gamma}_0(T);T,T_r)}{S_{21}(T)S_{12}(T) + S_{22}(T)D(\widetilde{\Gamma}_0(T);T,T_r)} \tag{12}$$

where the auxiliary function $D(\widetilde{\Gamma}_0(T); T, T_r)$ is given by

$$D = S_{11}(T_r) - S_{11}(T) + \frac{S_{21}(T_r)S_{12}(T_r)\widetilde{\Gamma}_0(T)}{1 - S_{22}(T_r)\widetilde{\Gamma}_0(T)}$$

In view of the approximations that will follow, with a bit of algebra the above equation can be recast in the following form:

$$\Gamma_0(T) = \frac{1}{\alpha(T)}\widetilde{\Gamma}_0(T)A(\widetilde{\Gamma}_0, S_{11}, S_{22}, S_{21}S_{12}, T_r; T) \quad (13a)$$

$$\alpha(T) = \frac{S_{21}(T)S_{12}(T)}{S_{21}(T_r)S_{12}(T_r)} \quad (13b)$$

$$A = \frac{1+B}{1 + CS_{22}(T)\widetilde{\Gamma}_0(T)} \quad (13c)$$

where we defined

$$B = -\frac{\Delta S_{11}}{S_{21}(T_r)S_{12}(T_r)\widetilde{\Gamma}_0(T)}(1 - S_{22}(T_r)\widetilde{\Gamma}_0(T))$$

$$C = B\frac{S_{21}(T_r)S_{12}(T_r)}{S_{21}(T)S_{12}(T)} + \frac{\Delta S_{22}}{S_{22}(T_r)} - \frac{\Delta(S_{21}S_{12})}{S_{21}(T_r)S_{12}(T_r)}$$

and $\Delta S_{ii} = S_{ii}(T) - S_{ii}(T_r)$ and $\Delta(S_{21}S_{12}) = S_{21}(T)S_{12}(T) - S_{21}(T_r)S_{12}(T_r)$ reflect the temperature variations of S_{11}, S_{22} and $S_{21}S_{12}$.

In principle, Eq.s (13) can be used in Eq. (1) to obtain Z. Among the various factors which yield Γ_0, $\widetilde{\Gamma}_0$ has been already derived and $u(\widetilde{\Gamma}_m)$ evaluated. We now discuss the multiplicative factor A. During room temperature calibrations, we found $|S_{11}|$ and $|S_{22}|$ to be quite generally no more than 10% of $|S_{21}S_{12}|$, which is instead of the same order of $|\widetilde{\Gamma}_0| \simeq 1$ since we are focused on highly conductive samples. Moreover, the analysis of the frequency dependence of their phases shows that the main VSWR contribution to $|S_{11}|$ comes from the cable segment near the entrance of the cryostat, where the coaxial feedthrough is located. Since this cable end is thermally anchored to T_r, we do not expect $|S_{11}|$ to change by more than 10% for any variation of the temperature profile of the whole cable. In reciprocal, weakly lossy two-port networks, $|S_{11}| \simeq |S_{22}|$ [25] so that we expect the same behaviour for $|S_{22}|$. In addition, by measuring Γ_m at the minimum cryogenic temperature T_{min} at which $\Gamma_0 \simeq -1$ (see Sec. II and V-A), and assuming $S_{ii}(T_{min}) \simeq S_{ii}(T_r)$, by inverting Eq.(10) one can obtain a rough, worst-case estimate for $S_{21}(T_{min})S_{12}(T_{min})$ indicating that also $S_{21}S_{12}$ does not change by more than 10%. Thus $|S_{11}(T_r) - S_{11}(T)| \simeq 10^{-2}|S_{21}S_{12}\widetilde{\Gamma}_0|$, $|S_{22}\widetilde{\Gamma}_0| \simeq 0.1$, $|\Delta S_{22}/S_{22}| \simeq 0.1$ and $|\Delta(S_{21}S_{12})/(S_{21}S_{12})| \simeq 0.1$.

As a consequence, one finds $A = 1 + \delta A$ with $|\delta A| \ll 1$, so that A, which cannot be fully evaluated since the scattering coefficients at cryogenic T are not available, can be taken $\simeq 1$. The uncertainty $u(A)$ introduced by the latter approximation can be evaluated using the above written estimates for the moduli of the various coefficients. It can be shown that $u(|A|) = 0.03$. Assuming the worst case scenario of generic uncorrelated phases for all the complex quantities appearing in A, the uncertainty on its phase can be derived, obtaining $u(Arg(A)) = 0.03$ rad.

By taking $A = 1$ in Eq. (13a), it can be seen that Γ_0 differs from the measured $\widetilde{\Gamma}_0$ only by the multiplicative complex coefficient $\alpha^{-1}(\nu, T) = S_{21}(T_r)S_{12}(T_r)/(S_{21}(T)S_{12}(T))$. Hence, not surprisingly, the main contribution to the deviation between Γ_0 and $\widetilde{\Gamma}_0$ originates from the forward/reverse transmission of the internal cable: as discussed later, this occurs mainly in terms of phase contribution, due to the temperature-induced changes in length.

This coefficient depends in a nontrivial way upon the whole temperature profile of the cable so that no practical measurement of it is possible. A rough estimate of its variation, based on the numerical figures above provided, yield a relative variation with temperature $|\Delta\alpha|/|\alpha| \simeq 0.1$, to be compared with the reference value $\alpha(T_r) = 1$. Nevertheless, when performing measurements at low $T \lesssim 100$ K, it is reasonable to expect that $\alpha(T)$ is almost constant when varying the temperature of the sample of a few Kelvin (for an experimental check, see Sec. V-A); in fact, the cable is thermally constrained at T_r at the entrance of the cryostat, so that the temperature profile of the cable changes only slightly for such small variations of the temperature of the sample. If this is the case, although $\widetilde{\Gamma}_0(\nu)$ is essentially different from $\Gamma_0(\nu)$ because of the dominant contribution of $\alpha(T) \neq 1$ (see Eq. (13a)), the ratios of $\widetilde{\Gamma}_0(\nu)$ are good approximations to the ratios of the corresponding $\Gamma_0(\nu)$. Indeed, considering two distinct but not too far temperatures T_1 and T_2, using Eq. (13a), one obtains:

$$\frac{\Gamma_0(\nu; T_1)}{\Gamma_0(\nu; T_2)} = \frac{\widetilde{\Gamma}_0(\nu; T_1)}{\widetilde{\Gamma}_0(\nu; T_2)}\frac{A(T_1)}{A(T_2)}\frac{\alpha(T_2)}{\alpha(T_1)} \quad (14)$$

It is possible to check that, even if the deviation of α from unity can be as high as 10%, the *ratio* $\alpha(T_2)/\alpha(T_1)$ can yield a smaller deviation from unity, down to a few percent (this point will be extensively discussed in the following). Since the *variations* of Z depend on the *ratios* of the reflection coefficients only, we anticipate that, to a very good approximation, they are less affected by incomplete calibration, as it will be shown in the following Sec. IV-C.

C. Obtaining variations of $Z(\nu)$

In this paragraph we show that the ratio of two $\Gamma_0(\nu)$ determined at two different temperatures or magnetic fields is related to the corresponding difference of impedances. Some approximations are needed which we will discuss in the next section. We first consider only temperature variations and then we will extend our conclusions to the case of varying magnetic field.

Let's consider the difference between two curves of $Z(\nu)$ at two different values of the temperature T_1 and T_2. Making use of Eq. (1), we can write

$$\Delta Z(\nu; T_1, T_2) \doteq Z(\nu; T_1) - Z(\nu; T_2) =$$

$$Z_0\left(\frac{1+\Gamma_0(\nu;T_1)}{1-\Gamma_0(\nu;T_1)} - \frac{1+\Gamma_0(\nu;T_2)}{1-\Gamma_0(\nu;T_2)}\right) \simeq Z_0\frac{1 - \frac{\Gamma_0(\nu;T_1)}{\Gamma_0(\nu;T_2)}}{1 + \frac{\Gamma_0(\nu;T_1)}{\Gamma_0(\nu;T_2)}} \quad (15)$$

We write $\Gamma_0(\nu; T_2) = -1 + \delta\Gamma_2$. The last approximate equality in Eq. (15) becomes exact when $\delta\Gamma_2 = 0$; the deviations are $\propto \delta\Gamma_2$. As discussed in Sec.V-A, in the practical case here

of interest, $|\delta\Gamma_2| \ll 1$. As a simple estimate, using the same two–fluid model as in Sec. II, with $x_n \leq 0.9$, $|\delta\Gamma_2| < 10^{-4}$ at $\nu = 20$ GHz, negligible with respect to the uncertainties on $\widetilde{\Gamma}_m$ and A.

We now introduce the notation $\Delta\phi_j(T_1;T_2) \doteq Arg[Q_j(T_1)] - Arg[Q_j(T_2)]$, where $j = 0$, $\widetilde{m}$, α and A refers to Γ_0, $\widetilde{\Gamma}_m$, α and A, respectively.

If $\Delta\phi_0(\nu) \ll 1$ then $Re\frac{\Gamma_0(\nu;T_1)}{\Gamma_0(\nu;T_2)} \simeq \left|\frac{\Gamma_0(\nu;T_1)}{\Gamma_0(\nu;T_2)}\right|$ and $Im\frac{\Gamma_0(\nu;T_1)}{\Gamma_0(\nu;T_2)} \simeq \left|\frac{\Gamma_0(\nu;T_1)}{\Gamma_0(\nu;T_2)}\right|\Delta\phi_0$ hold. This approximation, with the typical values of $\Delta\phi_0 \leq 0.1$ rad (see Sec. V-A), gives $u(\Delta R)/\Delta R = u(\Delta X)/\Delta X \leq 5\cdot 10^{-3}$, again negligible with respect to the uncertainties on $\widetilde{\Gamma}_m$ and A. In this case from Eq. (15) one has:

$$\Delta R(\nu;T_1,T_2) \simeq Z_0 \frac{1-|\frac{\Gamma_0(\nu;T_1)}{\Gamma_0(\nu;T_2)}|}{1+|\frac{\Gamma_0(\nu;T_1)}{\Gamma_0(\nu;T_2)}|} \tag{16}$$

$$\Delta X(\nu;T_1,T_2) \simeq -2Z_0 \frac{|\frac{\Gamma_0(\nu;T_1)}{\Gamma_0(\nu;T_2)}|}{\left(1+|\frac{\Gamma_0(\nu;T_1)}{\Gamma_0(\nu;T_2)}|\right)^2}\Delta\phi_0 \tag{17}$$

We stress that ΔR depends only on the ratio of the moduli of the reflection coefficients and not upon the phase variations. In this way the determination of ΔR requires information about $|\Gamma_0(T_1)/\Gamma_0(T_2)|$ only, while obtaining ΔX requires also the knowledge of $\Delta\phi_0$.

If we now make use of Eq. (14) to determine the ratio $|\Gamma_0(T_1)/\Gamma_0(T_2)|$ from the measured reflection coefficients, the above expressions for ΔR and ΔX can be rewritten as follows.

Using Eq. (14), with $|A(T_1)/A(T_2)| = 1$ and $|\alpha(\nu;T_1)| \simeq |\alpha(\nu;T_2)|$ (small T variations), so that $|\Gamma_0(T_1)/\Gamma_0(T_2)| \simeq |\widetilde{\Gamma}_m(T_1)/\widetilde{\Gamma}_m(T_2)|$, Eq. (16) finally yields

$$\Delta R(\nu;T) \simeq Z_0 \frac{1-\frac{|\widetilde{\Gamma}_0(\nu;T_1)|}{|\widetilde{\Gamma}_0(\nu;T_2)|}}{1+\frac{|\widetilde{\Gamma}_0(\nu;T_1)|}{|\widetilde{\Gamma}_0(\nu;T_2)|}} \tag{18}$$

Taking $\Delta\phi_A \ll \Delta\phi_0$, in the additional case $\Delta\phi_\alpha \ll \Delta\phi_0$ (see below) so that $\Delta\phi_0 \simeq \Delta\phi_{\widetilde{m}}$, Eq. (17) gives:

$$\Delta X(\nu;T) \simeq -2Z_0 \frac{\frac{|\widetilde{\Gamma}_0(\nu;T_1)|}{|\widetilde{\Gamma}_0(\nu;T_2)|}}{\left(1+\frac{|\widetilde{\Gamma}_0(\nu;T_1)|}{|\widetilde{\Gamma}_0(\nu;T_2)|}\right)^2}\Delta\phi_{\widetilde{m}} \tag{19}$$

The corresponding relative uncertainties are:

$$\frac{u(\Delta R)}{\Delta R} = \frac{2|\frac{\Gamma_0(T_1)}{\Gamma_0(T_2)}|}{1-\left(|\frac{\Gamma_0(T_1)}{\Gamma_0(T_2)}|\right)^2}\frac{u(|\frac{\Gamma_0(T_1)}{\Gamma_0(T_2)}|)}{|\frac{\Gamma_0(T_1)}{\Gamma_0(T_2)}|} \tag{20}$$

$$\frac{u(\Delta X)}{\Delta X} = \left[\left[\frac{1-|\frac{\Gamma_0(T_1)}{\Gamma_0(T_2)}|}{1+|\frac{\Gamma_0(T_1)}{\Gamma_0(T_2)}|}\frac{u(|\frac{\Gamma_0(T_1)}{\Gamma_0(T_2)}|)}{|\frac{\Gamma_0(T_1)}{\Gamma_0(T_2)}|}\right]^2 + \left[\frac{u(\Delta\phi_0)}{\Delta\phi_0}\right]^2\right]^{\frac{1}{2}} \tag{21}$$

where $u(|\Gamma_0(T_1)/\Gamma_0(T_2)|)$ and $u(\Delta_0)$ must be evaluated starting from Eq. (14). In the above, it can be seen that the uncertainties depend also on the actual values of $\Gamma_0(T_1)/\Gamma_0(T_2)$, i.e. on the value of the $Z(T_2)$ being measured [20].

From Eq. (14), we get:

$$\frac{u(|\frac{\Gamma_0(T_1)}{\Gamma_0(T_2)}|)}{|\frac{\Gamma_0(T_1)}{\Gamma_0(T_2)}|} = \left[\left(\frac{u(|\widetilde{\Gamma}_m(T_1)|)}{|\widetilde{\Gamma}_m(T_1)|}\right)^2 + \left(\frac{u(|\widetilde{\Gamma}_m(T_2)|)}{|\widetilde{\Gamma}_m(T_2)|}\right)^2 + \left(\frac{u(|A(T_1)|)}{|A(T_1)|}\right)^2 + \left(\frac{u(|A(T_2)|)}{|A(T_2)|}\right)^2 + \left(\frac{u(|\alpha(T_2)/\alpha(T_1)|)}{|\alpha(T_2)/\alpha(T_1)|}\right)^2\right]^{\frac{1}{2}} \tag{22}$$

$$u(\Delta\phi_0) = \left[u(\Delta\phi_{\widetilde{m}}(T_1;T_2))^2 + u(\Delta\phi_A(T_1;T_2))^2 + u(\Delta\phi_\alpha(T_1;T_2))^2\right]^{\frac{1}{2}} \tag{23}$$

where in Eq. (22) $u(|\widetilde{\Gamma}_m|)$ is a measurement uncertainty, $u(|A|)$ and $u(|\alpha(T_2)/\alpha(T_1)|)$ are approximation uncertainties. In particular, as extensively discussed, $|\alpha(T_2)/\alpha(T_1)| = 1 + \delta(|\alpha(T_2)/\alpha(T_1)|)$, with $\delta(...) \ll 1$ comes from the weak temperature dependence of $|\alpha(T)|$. The same arguments hold for the corresponding terms in Eq. (23).

Formulae 18–23 are the main result of this paper. They relate the variation of impedance between two different temperatures to the measured quantities. Through these formulae, in fact, once a temperature T_{ref} at which $\Gamma_0 \simeq -1$ is fixed, the differences $\Delta Z(\nu;T) \doteq Z(\nu;T) - Z(\nu;T_{ref})$ for each temperature T can be obtained, together with their uncertainties. In this case, $\widetilde{\Gamma}_m(T_{ref})$ and $A(T_{ref})$ have the role of reference values, so that their uncertainties qualify as systematic. Moreover, once all the ΔZ are known, if a temperature T^* exists for which the curve $Z(\nu;T^*)$ is theoretically predictable or experimentally known, absolute values of $Z(\nu;T)$ can be extracted.

The procedure can be easily extended to the case of measurements as a function of the applied magnetic field at a fixed temperature T_0 (field sweeps). In this case, $\Delta Z = \Delta Z(\nu;H) \doteq Z(\nu;H,T_0) - Z(\nu;H_{ref},T_0)$ and the values of $\Delta R(\nu,H)$ and $\Delta X(\nu,H)$ are obtained with the same expressions as in Eq.s (18), (19) by replacing the temperature dependence with the magnetic field dependence. With respect to measurements as a function of temperature, there is the additional advantage that the response of the cable is not expected to vary by applying an external magnetic field. This implies that $\alpha(\nu)$ remains constant among measurements at different magnetic fields, provided that the whole cable has reached its equilibrium temperature profile. As a result, the condition $\alpha(\nu;H) = \alpha(\nu;H_{ref})$ required in Eq.s (18), (19) is exactly, instead of approximately, satisfied. Moreover, making the approximation $A(H_1,T_0)/A(H_2,T_0) \simeq 1$ involves a smaller error, since the two coefficients A differ only through their dependence on $\widetilde{\Gamma}_m(H_i,T_0)$.

V. Experimental results

A. Check of the validity of the approximations

We here discuss the validity of the approximations introduced in the previous section to obtain Eq.s (18), (19). We will use measurements performed on two thin ($d \simeq 150$ nm), square (l = 5 mm) MgB_2 films, grown on sapphire substrates

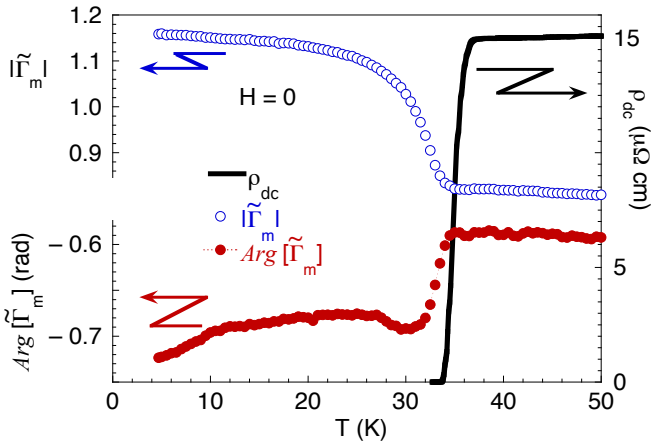

Fig. 4. Left hand scales: modulus (blue empty circles) and phase (red full circles) of $\widetilde{\Gamma}_0(\nu, T)$ at fixed frequency $\nu = 17.5$ GHz as a function of the temperature. Right hand scale, continuous black line: DC resistivity ρ_{dc} of the same sample. All measurements taken at zero field in sample I.

[40], and independent DC measurements and theoretical predictions. Two of these approximations concern Γ_0: *(i)* that it exists a pair of values {H,T} for which $\Gamma_0(H, T, \nu) \simeq -1$, and *(ii)* that the variations of $Arg[\Gamma_0]$ as a function of T and H are small. Two more approximations concern α: *(iii)* that $|\alpha| \simeq$ const with small T variations, and *(iv)* that $\Delta\phi_A - \Delta\phi_\alpha \ll \Delta\phi_0$.

In order to identify the {H,T} values for which $\Gamma_0(\nu) \simeq -1$ and for which R and/or X are known, we recall that at $H = 0$ and sufficiently low T one has $R, X \ll Z_0$, and then $\Gamma_0(\nu) \simeq -1$. As discussed in Sec. II, above T_c the resistivity ρ_n is real and $X \simeq 0$. We note that the sapphire substrate does not yield anomalous substrate effects [41].

The second approximation can be checked by measuring the temperature variations of the phase of $\widetilde{\Gamma}_m$. In Fig. 4 we report $Arg[\widetilde{\Gamma}_m]$ as a function of T for $H = 0$ and $\nu = 17.5$ GHz. Measurements refer to sample I. The overall behaviour is composed by a rather abrupt feature, located just below T_c, over a smooth background. Since the phase of Γ_0 is expected to be constant, as a function of T, both above T_c (where Z and thus Γ_0 are real) and sufficiently below T_c (where, as discussed above, $Arg[\Gamma_0] \simeq \pi$), the smooth background originates from variations of $Arg[A] - Arg[\alpha]$ and the abrupt feature from variations of Γ_0. The feature of $Arg[\Gamma_0]$ can be easily understood on general grounds: in fact, $Arg[\Gamma_0] \neq 0, \pi$ only if X is comparable with Z_0, which can happen only at temperatures slightly below T_c, since deep in the superconducting state $X \ll Z_0$. Similar results are obtained also with an applied magnetic field. The measurements give $\Delta\phi_0 \leq 0.1$ rad, so that the approximation $\Delta\phi_0 \ll 1$ is reasonably fulfilled for all T and H.

We show now that $|\alpha| \simeq$ const. Fig. 4 reports the measured DC resistivity on sample I, and $|\widetilde{\Gamma}_m|$ at 17.5 GHz. Above T_c, since ρ is real and frequency–independent, Z is real, and Γ_0 is real and frequency independent. Moreover, for 35K$< T <$ 45K ρ_{DC} is almost T–independent, and so is Γ_0. We observe that $|\Gamma_m|$ is approximately constant between 45 K and 35 K, and at low T it changes little and it tends to saturate. This is consistent with the above discussion: above T_c, Γ_0 is almost independent on T; at low T, $|\Gamma_0| \simeq 1$. The small variations with T can then be ascribed to variations of $|\alpha(T)A(T)|$ and, since A changes by less than 3% in the worst case, the variation of $|\alpha(T)|$ turns out to be much smaller than the variations of $|\Gamma_0(T)|$, as required. Thus, R can be obtained from $|\Gamma_m|$.

The last approximation to be verified concerns the variations of $Arg[\alpha]$ and $Arg[A]$. It is evident from Fig. 4 that the abrupt variation of $Arg[\Gamma_0]$ at T_c is of the same order of magnitude as the variations of the smooth background, so that $|\Delta\phi_A - \Delta\phi_\alpha| \ll \Delta\phi_0$ does not hold: we cannot make use of Eq. (19) to get X from measurements as a function of temperature. This limitation is intrinsically eliminated when performing measurements at a fixed temperature as a function of the applied magnetic field (field sweeps), that allow for a determination of both the real and the imaginary part of ΔZ.

B. Obtaining the impedances

The practical method to determine the impedance Z proceeds as follows. We begin with the zero field case. First, we choose a reference temperature $T_{ref} \ll T_c$ with respect to which the variation of the impedance will be calculated, to satisfy the approximation in Eq. (15). Following the discussion of the previous subsection, the lower T_{ref}, the better Eq. (15) is satisfied. We then choose $T_{ref} = 4$ K for our MgB_2 samples.

In the present case where in fact, well within the resolution of the method, R(4 K) = 0, the differences $\Delta R(\nu; T, 0) = R(\nu; T, 0) - R(\nu; T_{ref}, 0)$ coincide with the absolute values.

For what concerns the field sweeps measurements we chose $H_{ref} = 0$ for all sweeps. In this case, when the temperature T_0 at which the field sweep is performed is close to T_c, the condition $\Gamma_0(\nu; T_0, H_{ref}) \simeq -1$ is not fully satisfied. Nevertheless, by using the values of $R(\nu; T, 0)$ obtained from the zero field data, we can estimate in no more than 5% the error made with the approximation contained in Eq. (15). Absolute values of R can again be obtained by using $R(0, T, \nu)$ from the zero–field data as obtained above.

To obtain absolute values of X we cannot make use of the zero field data: X cannot be extracted from such measurements due to the failure of the approximation $\Delta\phi_\alpha \ll \Delta\phi_0$. However we can drive the superconductors in the normal state by applying a strong magnetic field (above the so–called upper magnetic field, H_{c2}). In the normal state, since we are dealing with a thin film, X is expected to vanish: this general feature of superconductors gives the desired reference point to convert the differences $\Delta X(H, T_0, \nu)$ in absolute values.[2]

In Fig. 5a we report sample measurements taken in the MgB_2 thin film (sample I), normalized to Z_0, see Eq.s (18), (19). As discussed previously, it is not possible to obtain X as a function of the temperature. Fig. 5a reports R/Z_0. The typical broadening of the superconducting transition with the frequency is clearly observed, as well as the magnetic–field dependent broadening. This figure exemplifies the potential of the technique, in obtaining the variation of the surface

[2]In a bulk metal, one would have instead $R = X$. Also this property could in principle be exploited, depending on the geometry of the sample.

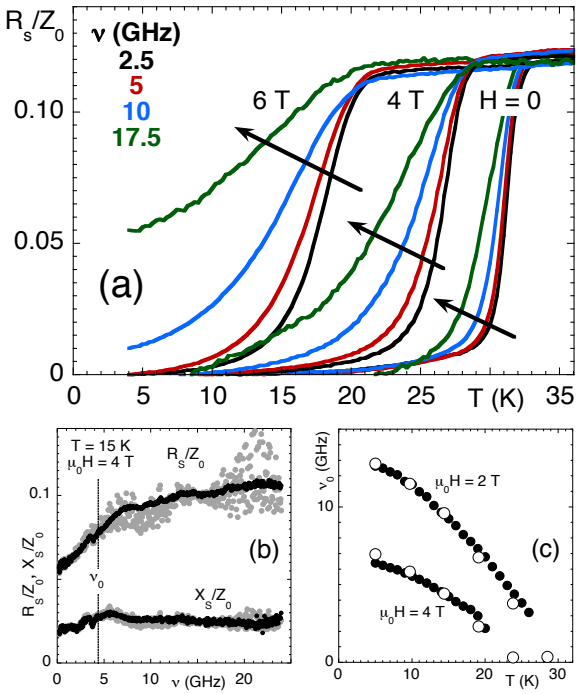

Fig. 5. (a) Surface impedance measurements normalized to Z_0, R/Z_0, in the superconducting MgB_2 thin film, sample I, taken at $\mu_0 H = 0$, 4 T and 6 T, at several frequencies as a function of the temperature. For each field, the frequency increases along the arrow. (b) R/Z_0 and X/Z_0 as a function of the frequency, at fixed T=15 K and field $\mu_0 H = 4.0$ T in sample II. Black symbols: data obtained by using the calibration procedure obtained in this paper; grey symbols: data obtained by using the so–called "short–only" calibration (see text). (c) Characteristic frequency $\nu_0(T)$ obtained in sample II at two different fields (full symbols) as compared to literature data obtained at 9.3 GHz [43] (open symbols).

impedance in an extended range of frequency, temperature, and magnetic field. In order to better demonstrate the advantages of the technique, we present further data taken in sample II, where a more extensive frequency study has been performed. In Fig. 5b, we report measurements of R/Z_0 and X/Z_0 at fixed T=15 K and field $\mu_0 H$=4 T. This Figure allows to compare the improvement brought by our calibration technique over the "short–only" calibration: we report the same data after our improved calibration (black symbols) and after the short–only procedure (gray symbols). The improvement in the dispersion of the data is apparent.

We now shortly compare our results with those (few) existing in the literature. In a magnetic field, quantized flux lines exist in the superconductor [31]. Their behavior is responsible for the nontrivial frequency dependence of the surface impedance [31], [42]. In particular, a crossover frequency ν_0 exists: it approximately coincides with the midpoint of $R(H)$ or the peak of $X(H)$ (see Fig.5b), and it marks a change of dynamics of the flux lines [42]. Fig. 5c reports a comparison of the data for ν_0 obtained by the present technique, and data derived from a more conventional resonator technique at 9.3 GHz [43]. While the exact overlap of the two sets of data may be coincidental, it is clear that the data obtained with the Corbino disk compare nicely to the data obtained by other techniques.

VI. Conclusions

We have presented an improvement of the "short-only" approximated calibration technique for the Corbino disk technique, useful to obtain swept-frequency measurements of the surface impedance of superconducting thin films. The basic idea is to apply incremental calibration and approximations, using the available data for the check of the approximation themselves.

We have discussed the relation of the measurand, the surface impedance, with the material complex resistivity, and obtained properties useful in the calibration process. We have thoroughly discussed the uncertainties involved in the approximate calibration procedure here proposed. Finally, we have experimentally checked the approximations in the case of superconducting MgB_2 samples, and we have obtained data of the temperature and field variations of the surface impedance. Albeit far from metrological–grade measurements, the present approximate calibration represents one of the very few methods to obtain swept–frequency measurements in superconductors.

Acknowledgments

We thank C. Ferdeghini for the MgB_2 samples and C. Amabile for his help in the measurements on MgB_2.

References

[1] L. F. Chen, C. K. Ong, C. P. Neo, V. V. Varadan, V. K. Varadan, "Microwave Electronics: Measurement and Materials Characterization," John Wiley & Sons, Ltd, 2004.

[2] H. C. F. Martens, J. A. Reedijk, and H. B. Brom, "Measurement of the complex dielectric constant down to helium temperatures. I. Reflection method from 1 MHz to 20 GHz using an open ended coaxial line," Rev. Sci. Instrum., vol. 71, 2000, pp. 473–477.

[3] M. S. Boybay, Omar M. Ramahi, "Material Characterization Using Complementary Split-Ring Resonators," IEEE Trans. Instrum. Meas., vol. 61, Nov. 2012, pp. 3039–3046.

[4] M. Tofighi and A. S. Daryoush, "Biological Tissue Complex Permittivity Measured From S_{21} Error Analysis and Error Reduction by Reference Measurements," IEEE Trans. Instrum. Meas., vol. 58, 2009, pp. 2316–2327.

[5] F. Bordi, C. Cametti, and R. H. Colby, "Dielectric spectroscopy and conductivity of polyelectrolyte solutions," J. Phys.: Condens. Matter, vol. 16, Dec. 2004, pp. R1423–R1463.

[6] D. Bourreau, A. Péden, and S. Le Maguer, "A Quasi-Optical Free-Space Measurement Setup Without Time-Domain Gating for Material Characterization in the W-Band," IEEE Trans. Instrum. Meas., vol. 55, 2006, pp. 2022–2028.

[7] J. O. Curtis, "A durable laboratory apparatus for the measurement of soil dielectric properties," IEEE Trans. Instrum. Meas., vol. 50, 2001, pp.1364–1369.

[8] A. P. Gregory, R. N. Clarke, and M. G. Cox, "Traceable measurement of dielectric reference liquids over the temperature interval 10–50 °C using coaxial-line methods," Meas. Sci. Technol., vol. 20, Jul. 2009, p. 075106.

[9] P. Quéffélec, M. Le Floc'h, and P. Gelin, "New method for determining the permeability tensor of magnetized ferrites in a wide frequency range," *IEEE Trans. Microw. Theory Techn.*, vol. 48, 2000, pp. 1344–1351.

[10] A. Sharma, M. N. Afsar, "Accurate Permittivity and Permeability Measurement of Composite Broadband Absorbers at Microwave Frequencies," Instrumentation and Measurement Technology Conference (I2MTC) IEEE, 2011, pp. 1–6.

[11] J. Krupka and J. Mazierska, "Contactless Measurements of Resistivity of Semiconductor Wafers Employing Single-Post and Split-Post Dielectric-Resonator Techniques," IEEE Trans. Instrum. Meas., vol. 56, Oct. 2007, pp. 1839–1844.

[12] J.-Y. Chung, N. K. Nahar, L. Zhang, Y. Bayram, K. Sertel, and J. L. Volakis, "Broadband radio frequency conductivity measurement technique for engineered composites," IET Microwaves, Antennas and Propagation, vol. 6, 2012, pp. 371–376.

[13] J. Mollá, A. Ibarra, J. Margineda, J. M. Zamarro, and A. Hernandez, "Measurement System at Cryogenic Temperatures and Microwave Frequencies," IEEE Trans. Instrum. Meas., vol. 42, 1993, pp. 817–821.

[14] Z. We and L. E. Davis, "A method for determination of microwave surface impedance of high-T_c thick film and bulk superconductors," IEEE Trans. Instrum. Meas., vol. 43, 1994, pp. 532–535.

[15] H. Lue, J. Lue, and T. Tseng, "Microwave Penetration Depth Measurement for High T_c Superconductors by Dielectric Resonators," IEEE Trans. Instrum. Meas., vol. 51, 2002, pp. 433–439.

[16] N. Pompeo, K. Torokhtii, and E. Silva, "Dielectric Resonators for the Measurements of the Surface Impedance of Superconducting Films," Meas. Sci. Rev., vol.14, 2014, pp. 164–170, and references therein.

[17] J. C. Booth, D. H. Wu, and S. M. Anlage, "A broadband method for the measurement of thin films at microwave frequencies," Rev. Sci. Instrum., vol. 65, 1994, pp. 2082–2090.

[18] H. Kitano, T. Ohashi, and A. Maeda, "Broadband method for precise microwave spectroscopy of superconducting thin films near the critical temperature," Rev. Sci. Instrum., vol. 79, Jul. 2000, art. no. 074701.

[19] N. Tosoratti, R. Fastampa, M. Giura, V. Lenzi, S. Sarti, and E. Silva, "Two Techniques For Broadband Measurement Of The Surface Impedance Of High Critical Temperature Superconducting Thin Films," Int. J. Mod. Phys. B., vol. 14, 2000, pp. 2926–2931.

[20] M. Scheffler and M. Dressel, "Broadband microwave spectroscopy in Corbino geometry for temperatures down to 1.7 K," Rev. Sci. Instrum., vol. 76, 2005, art. no. 074702.

[21] M. Scheffler, M. Maximilian Felger, M. Thiemann, D. Hafner, K. Schlegel, M. Dressel, K. S. Ilin, M. Siegel, S. Seiro, C. Geibel, F. Steglich, "Broadband Corbino spectroscopy and stripline resonators to study the microwave properties of superconductors," Acta IMEKO, vol. 4, 2015, pp. 47–52.

[22] E. Silva, N. Pompeo, and S. Sarti, "Wideband microwave measurements in Nb/$Pd_{84}Ni_{16}$/Nb structures and comparison with thin Nb films," Supercond. Sci. Technol. , vol. 24, no. 2, 2011, art. no. 024018.

[23] E. Silva, N. Pompeo, K. Torokhtii, S. Sarti, "Cryogenic Microwave Wideband Measurements of Superconducting Thin Films", Proceedings of I2MTC, Pisa, May 11-14 (2015), in Instrumentation and Measurement Technology Conference (I2MTC), 2015 IEEE International, pp.358-363. doi: 10.1109/I2MTC.2015.7151294

[24] U. Kaatze, "Techniques for measuring the microwave dielectric properties of materials," Metrologia, vol. 47, Apr. 2010, pp. S91–S113.

[25] R. E. Collin, "Foundation for Microwave Engineering", McGraw-Hill International Editions, 1998.

[26] David M. Pozar, "Microwave engineering", John Wiley & Sons, Inc., 2012.

[27] S. Bakhtiari, S. I. Ganchev and R. Zoughi, "Analysis of radiation from an open-ended coaxial line into stratified dielectrics," IEEE Trans. Instrum. Meas., vol. 42, 1994, pp. 1261–1267.

[28] E. Silva, M. Lanucara, R. Marcon, "The effective surface resistance of superconductor/dielectric/metal structures," Supercond. Sci. Technol. , vol. 9, 1996, no. 11, pp. 934–941.

[29] N. Pompeo, R. Marcon, L. Méchin, and E. Silva, "Effective surface impedance of $YBa_2Cu_3O_{7-\delta}$ films on silicon substrates," Supercond. Sci. Technol. , vol. 18, no. 4, 2005, pp. 531–537.

[30] N. Pompeo, L. Muzzi, V. Galluzzi, R. Marcon, and E. Silva, "Measurements and removal of substrate effects on the microwave surface impedance of YBCO films on $SrTiO_3$," Supercond. Sci. Technol. , vol. 20, 2007, no. 10, pp. 1002–1008.

[31] M. J. Lancaster, "Passive Microwave Device Applications of High-Temperature Superconductors," Cambridge University Press, New York, 1997.

[32] L. Ranzani, L. Spietz, Z. Popovic, and J. Aumentado, "Two-port microwave calibration at millikelvin temperatures," Rev. Sci. Instrum., vol. 84, Mar. 2013, art. no. 034704.

[33] J.-H. Yeh and S. M. Anlage, "In situ broadband cryogenic calibration for two-port superconducting microwave resonators," Rev. Sci. Instrum., vol. 84, Mar. 2013, art. no. 034706.

[34] I. Farrance, R. Frenkel, "Uncertainty of Measurement: A Review of the Rules for Calculating Uncertainty Components through Functional Relationships," The Clinical Biochemist Reviews, vol. 33, 2012, pp. 49–75.

[35] P. da Silva Hack, C. S. ten Caten, "Measurement Uncertainty: Literature Review and Research Trends," IEEE Trans. Instrum. Meas., vol. 61, Aug. 2012, pp. 2116–2124.

[36] Agilent Technologies Inc., "Agilent 8510C Network Analyzer Data Sheet," 5091-8484E datasheet, vol. 56, July. 2006.

[37] N. Yannopoulou, P. Zimourtopoulos, "Total Differential Errors in One-Port Network Analyzer Measurements with Application to Antenna Impedance," Radioeng., vol. 16, June 2007, pp. 1–8.

[38] N. M. Ridler, M. J. Salter, "An approach to the treatment of uncertainty in complex S-parameter measurements," Metrologia, vol. 39, 2002, pp. 295-302.

[39] U. Stumper, T. Schrader, "Influence of Different Configurations of Non-ideal Calibration Standards on Vector Network Analyzer Performance," IEEE Trans. Instrum. Meas., vol. 61, July 2012, pp. 2034–2041.

[40] V. Ferrando, S. Amoruso, E. Bellingeri, R. Bruzzese, P. Manfrinetti, D. Marrè, N. Spinelli, R. Velotta, X. Wang, C. Ferdeghini, "Growth methods of c-axis oriented MgB_2 thin films by pulsed laser deposition," Supercond. Sci. Technol. , vol. 16, 2003, pp. 241–245.

[41] S. Sarti, C. Amabile, E. Silva, M. Giura, R. Fastampa, C. Ferdeghini, V. Ferrando, and C. Tarantini, "Dynamic regimes in MgB_2 probed by swept frequency microwave measurements," Phys. Rev. B, vol. 72, 2005, no. 2, art. no. 024542.

[42] N. Pompeo and E. Silva, "Reliable determination of vortex parameters from measurements of the microwave complex resistivity," Phys. Rev. B, vol. 78, 2008, art. no. 094503.

[43] A. Dulčić, D. Paar, M.Požek, G. V. M. Williams, S. Krämer, C. U. Jung, Min-Seok Park, and Sung-Ik Lee, "Magnetization and microwave study of superconducting MgB_2," Phys. Rev. B, vol. 66, 2002, art. no. 014505